Asian Journal of Chemistry; *Vol. 38, No. 5 (2026), 1170-1176*

ASIAN JOURNAL OF CHEMISTRY

https://doi.org/10.14233/ajchem.2026.35559

Effect of SiO_4^{2-}, Fe^{3+}, Mg^{2+} and Al^{3+} on Surface Hydration and Activation of Water Adsorbed on Apatite

M. KHALIL[1,2,*], FZ. MAAROUF[1], H. KHALIL[1], A. BELLAOUCHOU[2], S. BOUHLASSA[1] and M. HMAMOU[1]

[1]Laboratory of Applied Chemistry of Materials (LCAM), Faculty of Sciences, Mohammed V University, Rabat, Morocco
[2]Laboratory of Materials, Nanotechnology and Environment, Faculty of Sciences, Mohammed V University, P.O. Box.1014, Rabat, Morocco

*Corresponding author: E-mail: mariamkhalil47@gmail.com

Received: 2 January 2026 | *Accepted*: 12 March 2026 | *Published online*: 4 May 2026 | AJC-22341

The surface properties of apatite are crucial for its reactivity and release behaviour of phosphate in the soil. Apatite exhibits a crystalline structure that strongly influences its morphology and surface characteristics. The morphology of apatite occurs in various forms, including granular, massive and fibrous textures, which can influence its interaction with soil particles and nutrient availability. This property also reflects the pH at which the surface charge of apatite becomes neutral. The surface of apatite can be enriched or depleted in certain elements compared to its bulk composition due to weathering processes and interactions with soil microbes. In this work, the hydration and activation of water adsorbed on apatite surfaces in presence of SiO_4^{2-}, Fe^{3+}, Mg^{2+} and Al^{3+} were investigated. Using integrated spectroscopic, potentiometric and surface chemistry analyses, distinct hydration, activation pathways were identified, and the evolution of surface species was monitored as a function of pH and dopant composition. The results demonstrate that surface protonation states and ligand exchange processes play key roles in controlling apatite reactivity in complex natural systems.

Keywords: Surface properties, Morphology, Apatite, Hydration.

INTRODUCTION

Hydroxyapatite (HAP), a hexagonal calcium phosphate mineral, consists of a repeating unit cell containing 44 atoms and two interpenetrating frameworks composed of calcium phosphate and channel anions such as F^-, OH^- or Cl^-. The crystal lattice is defined by Ca^{2+} ions, while tetrahedral PO_4^{3-} groups occupy structural sites and form a three-dimensional network through corner-sharing oxygen atoms. Interconnected cages and channels aligned parallel to the hexagonal axis contribute to its characteristic framework [1]. Stoichiometric HAP exposes two principal crystallographic surfaces, the *a*- and *c*-planes, corresponding to lateral and cross-sectional faces, respectively. These surfaces differ in charge distribution and can selectively adsorb cations or anions depending on the surrounding aqueous environment [2,3].

At hydrated solid interfaces, water plays a central role in controlling hydrolysis, surface complexation, sorption and precipitation phenomena. Dissociation of water at the interface generates hydroxide and hydronium ions, thereby modifying surface charge, reactivity, ion transport and biochemical interactions [4,5]. During the early hydration stage, water molecules are weakly adsorbed through van der Waals forces and hydrogen bonding. With increasing hydration, these molecules become more strongly bound, forming an ordered hydration layer adjacent to the apatite surface [6,7]. This structured layer, often described as ice-like water, strongly influences particle dispersion, interfacial chemistry and surface activity [8,9].

At charged apatite surfaces, an electric double layer develops in which specifically adsorbed ions remain close to the surface while counterions diffuse into solution. This charge separation governs electrostatic interactions and many surface reactions [10,11]. Hydration of apatite is controlled by the balance between water-water and water-surface hydrogen bonding. Under alkaline conditions, the negatively charged *c*-plane preferentially attracts cations, while hydroxyl and phosphate groups interact strongly with polar water molecules, creating a more ordered and reactive hydration shell [12,13]. As the hydration proceeds, the initially ordered water structure becomes less stable and gradually transforms into a more disordered, bulk-like arrangement through continuous adsorption and dissolution processes [14,15].

Water associated with apatite surfaces can be classified into bound water directly interacting with the surface, intermediate water with partial structuring, and free bulk water with minimal surface interaction. Strongly bound and bridging water molecules stabilize interfacial networks, whereas intermediate water exists as mono-, dimeric- or chain-like species with distinct mobility and hydrogen-bonding behaviour [16, 17]. In biological and mineral systems, maturation of apatite is accompanied by transformation of unstable, hydrated non-apatitic domains into more ordered apatitic regions, thereby reducing structural disorder and surface reactivity [18,19].

The Ca/P ratio strongly influences HAP-water interactions and surface acid-base behaviour [20,21]. Calcium deficient apatite (Ca/P < 1.50) generally exhibits acidic properties, whereas stoichiometric or calcium-rich apatite (Ca/P > 1.67) behaves more basally while retaining acidic sites [22-24]. Surface hydroxylation also determines hydrophilicity, electrostatic properties and the thickness of the adsorbed water layer. Increasing hydroxyl group density enhances water uptake and promotes formation of compact hydration layers.

Studies also reported that the point of zero charge (PZC) and isoelectric point (IEP) of HAP depend on the composition and experimental conditions. For synthetic HAP in 0.1 M KNO_3, the PZC decreases from 6.1 to 4.1 as solid-to-solution ratio changes from 1:100 to 1:500, whereas the IEP is mainly governed by the intrinsic surface chemistry [25,26]. Surface interaction with atmospheric CO_2 can generate carbonate species, shifting neutrality toward lower pH and decreasing the PZC from 8.65 to 7.05 [27,28]. In substituted apatite systems, incorporation of ions such as SiO_4, Fe, Mg and Al introduces surface heterogeneity that modifies hydration structure, activation states and the charge behaviour. Understanding these effects is essential for interpreting surface acidity, interfacial reactivity and mineral behaviour in complex natural environments.

EXPERIMENTAL

Chemical reagents of analytical grade were used without further purification. The experiments were undertaken using sodium hydroxide (NaOH, 99%), nitric acid (HNO_3, 37%) and sodium chloride (NaCl, 99%), along with distilled water.

Natural fluorapatite, with the chemical formula $Ca_{10}(PO_4)_6F_2$, is the principal component of phosphate rock, accounting for nearly 90 wt.%. The remaining fraction consists of associated minerals such as calcite, dolomite, quartz, amorphous silica, and organic matter. In addition to a high P_2O_5 content (31.51 wt.%), the samples contain significant CaO and SiO_2, along with minor constituents including F, MgO, Al_2O_3, Fe_2O_3 and TiO_2, present either within the apatite lattice or as mineral inclusions [29-32].

To assess the hydration effect, phosphate rocks were suspended in water medium, at varying durations (t_{hy}), while the activation process was carried out with suspending hydrated samples at specific pH and different durations (t_{ac}). The experimental process used to develop the acid- and alkali-activated apatite involves a multi-step analysis through characterisation techniques using energy dispersive X-ray spectroscopy coupled with scanning electron microscopy (EDX-SEM) (Jeol JSM-IT100 InTouchScope™) [33,34].

After phosphate activation, the resulting solid and liquid phases were examined to understand the water interactions, particularly hydration mechanisms and surface behaviour. Surface characterization was carried out using a batch equilibration method to determine the point of zero charge (PZC) and isoelectric point (IEP) [35]. This involved monitoring the pH of phosphate suspensions in 0.05 M HNO_3 or NaOH at the ambient temperature. In addition, the effect of hydration and activation time on surface properties was investigated using 20-25 mL HAP suspensions at a concentration of 0.2 g/L.

General procedure: Surface ionisation of HAP was investigated by a potentiometric protonation/deprotonation technique using phosphate material. All experiments were carried out at ambient temperature in batch mode using 20-25 mL suspensions containing 0.2 g/L apatite. After shaking the slurries, the final pH (pH_f) of the suspensions was measured. The H^+/OH^- exchange behaviour of HAP was evaluated by examining the effects of pH, hydration time and activation period. The experimental data were used to determine the point of zero charge (PZC) and isoelectric point (IEP). For this purpose, the initial pH (pH_i) and final pH (pH_f) of the suspension were analysed as functions of hydration time (T_{hy}) and activation time (T_{ac}). The variation, $\Delta pH = pH_f - pH_i$, was studied against T_{ac} at hydration times ranging from 2 to 72 h, while activation time varied from 0 to approximately 3 h. The batch experiments were conducted in glass flasks containing 25 mL of phosphate suspension. The non-linear $pH = f(T_{ac})$ curves obtained at fixed T_{hy} were fitted using a third-order equation ($R^2 > 95\%$) and the derived functions were used to determine $dpH/dT_{ac} = f(T_{ac})$ at constant pH.

RESULTS AND DISCUSSION

Phosphate rock is mainly composed of apatite (≈90 wt.%), while the remaining fraction consists of associated minerals such as calcite, dolomite, quartz, amorphous silica, and organic matter. Besides a high P_2O_5 content (31.51 wt.%), substantial amounts of CaO and SiO_2 are present. Minor constituents such as F, MgO, Al_2O_3, Fe_2O_3 and TiO_2 also occur either within the apatite lattice or as mineral inclusions. Owing to this multicomponent composition, the material exhibits structural features comparable to slag, glass or ceramic systems, with partially crystalline to amorphous characteristics [29-32].

Variations of atomic composition with hydration and activation process: The EDS spectra (Fig. 1) revealed the main elemental peaks of Ca, P, O, F and Si. After 2 h of hydration, the sample showed relatively high calcium and phosphorus contents, with a Ca/P ratio of 1.28, lower than the stoichiometric value for apatite (1.67). After a 24 h activation period, a noticeable decrease in Ca and P content was observed along with an increase in oxygen concentration. This compositional change was accompanied by improved morphological organisation and the appearance of more defined crystals, suggesting dissolution-reprecipitation processes and progressive crystal growth.

After 72 h of hydration, the composition became more stable, with a Ca/P ratio of 1.08 and nearly constant oxygen content. This stabilization was accompanied by a more homogeneous morphology composed of larger and well-developed particles, indicating an advanced stage of crystallization.

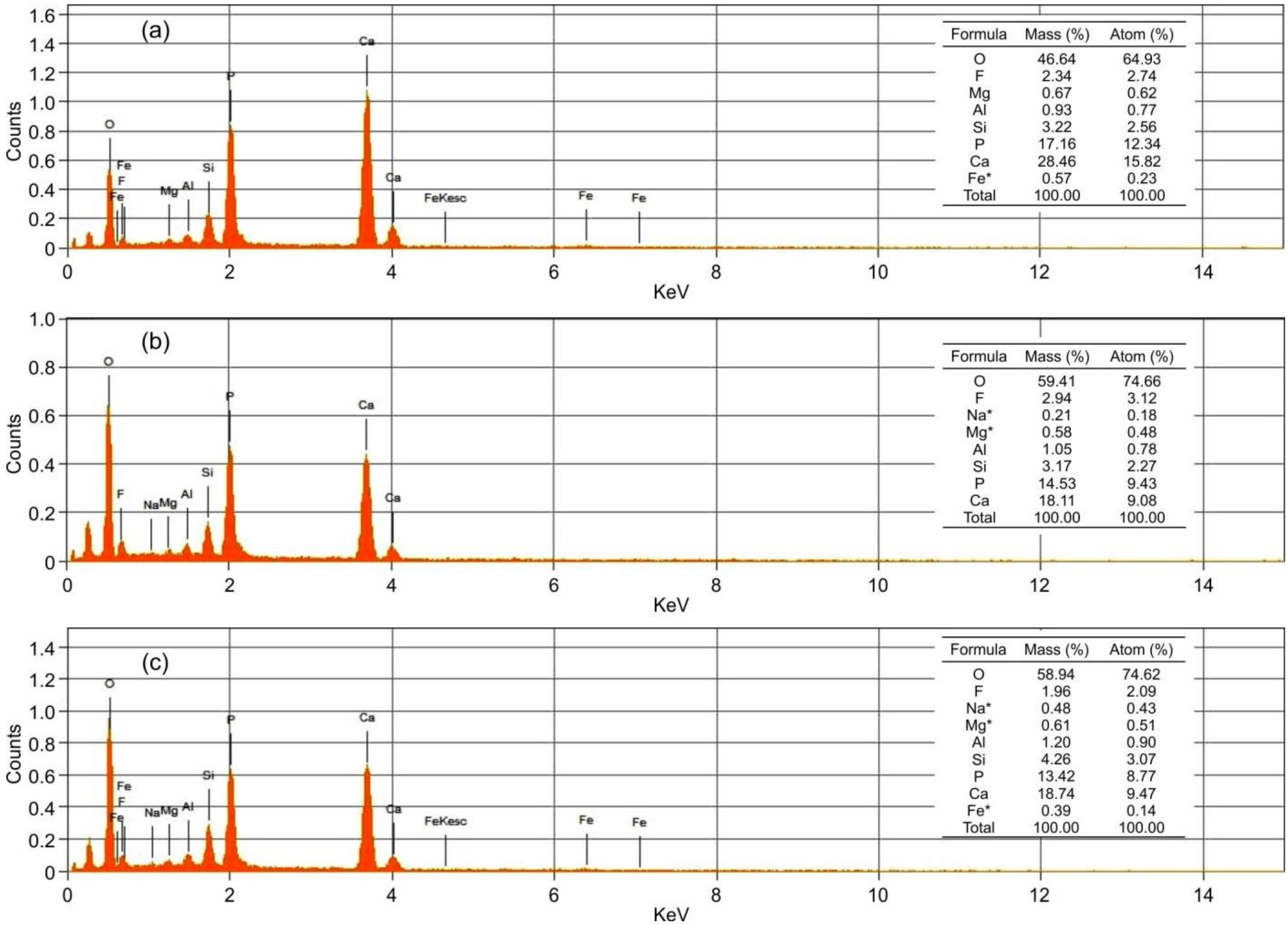

Fig. 1. EDS spectra of varied atomic composition with hydration and activation process at m = 0.2 g/L: (a,b) hydration 2 h; (c,d) hydration 24 h, activation of 10 min to 3 days; (e,f) hydration 72 h

The morphology of apatite powder hydrated for 2, 24 and 72 h and subsequently activated for 10 min to 3.5 h was examined by SEM (Fig. 2). The results showed that increasing hydration time progressively promoted apatite crystallisation, leading to a gradual transformation from an amorphous or semi-crystalline phase to a more ordered crystalline structure. Moreover, surface activation further accelerated this reorganization and crystal growth process.

Potentiometric analysis demonstrated that the isoelectric point (IEP) of apatite changed with hydration and activation time. The IEP was obtained from the intersection of $\Delta pH = f(pH)$ curves recorded at different hydration periods, while the point

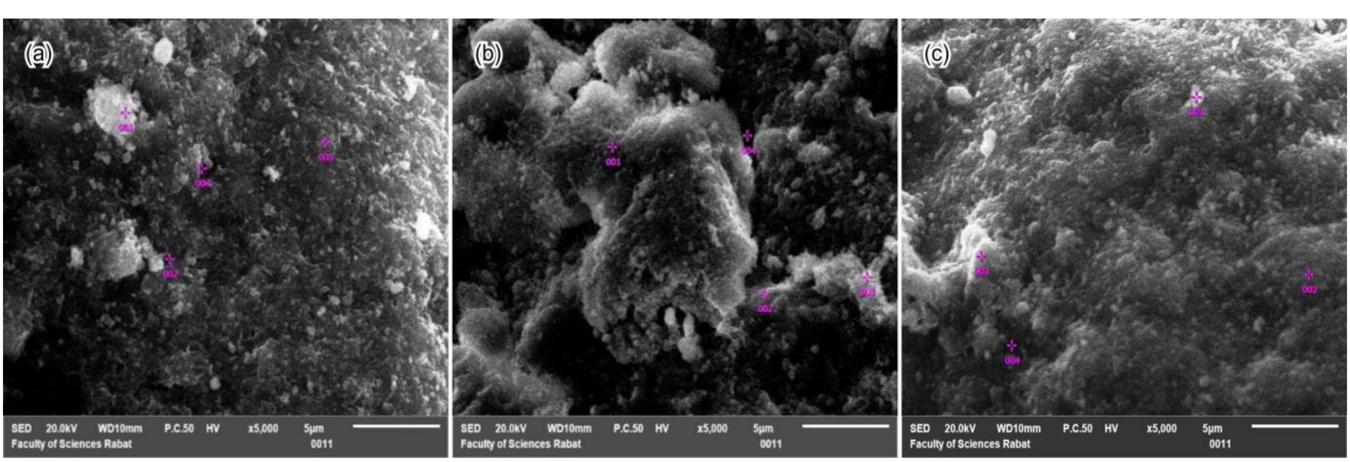

Fig. 2. Morphological images of apatite m = 0.2 g/L powder particles hydrated for (a) hydration 2 h; (b) hydration 24 h, activation of 10 min to 3 days; (c) hydration 72 h

of zero charge (PZC) corresponded to $\Delta pH = 0$. These results suggest that surface charging was mainly controlled by a physisorption process occurring at the external surface. Fig. 3 illustrates the variation of ΔpH as a function of pH for the apatite suspension (0.2 g/L) at hydration times (T_{hy}) of 2, 6, 12, and 24 h. The marked dependence of ΔpH on solution pH confirmed that the phosphate surface underwent progressive changes in protonation/deprotonation behaviour during hydration. Under the investigated conditions, both hydration and activation influenced the IEP, indicating continuous modification of the surface chemical environment. Initially, the IEP was close to pH 4 and gradually shifted toward pH 6 as hydration proceeded, whereas complete equilibrium required several weeks [36]. Lower ΔpH values were generally observed for activation times $\leq$ 3 h.

The displacement of IEP values was attributed to the dissolution-reprecipitation phenomena, surface proton transfer and activation of oxide phases associated with the phosphate matrix. Several characteristic IEP values were consistent with the presence of accessory minerals and the values of 9.2 ± 0.2 and 9.9 ± 0.2 were assigned to hematite (Fe_2O_3) and alumina (Al_2O_3), respectively [37]. An IEP of 3.8 ± 0.1 observed at short hydration time was associated with silica, while values near 4.0-4.2 corresponded to montmorillonite and kaolinite [38,39].

At T_{hy} = 12 h, an IEP/PZC value of 7.6 ± 0.1 suggested contributions from kaolinite, mixed oxides TiO_2-SiO_2-Al_2O_3), goethite (FeOOH) or Fe(III) hydroxide. A value of 8.4 ± 0.2 was linked to phyllosilicate phases, whereas an average IEP of 8.9 ± 0.2 was attributed to boehmite and illite minerals. The higher values around pH 10.2 were characteristic of serpentine, while unstable points near 5.4 ± 0.3 for T_{hy} = 2-12 h were related to rutile (TiO_2). Additional IEP values of 6.7 ± 0.3 and 7.3 ± 0.2 were assigned to octacalcium phosphate and lepidocrocite (γ-FeOOH), respectively [40,41]. These results confirmed that hydration and activation progressively altered the surface charge behaviour of apatite through restructuring of the interface and exposure of different mineral components.

To evaluate the effect of prolonged aging, the variation of ΔpH as a function of pH was examined at hydration times (T_{hy}) of 40 and 72 h under different activation conditions (Fig. 4). The results showed significant pH-dependent changes, particularly within the pH range of 6.5-10.5, indicating continued evolution of the apatite surface during long hydration periods.

At T_{hy} = 40 h, an isoelectric point (IEP) near pH 5.7 was observed, which can be attributed to TiO_2, consistent with literature reports. An IEP of 6.6 ± 0.2, detected at both 40 and 72 h, was associated with octacalcium phosphate. Another point near pH 8 did not correspond to a single well-defined mineral phase, but similar values (8.2 ± 0.2) have been reported

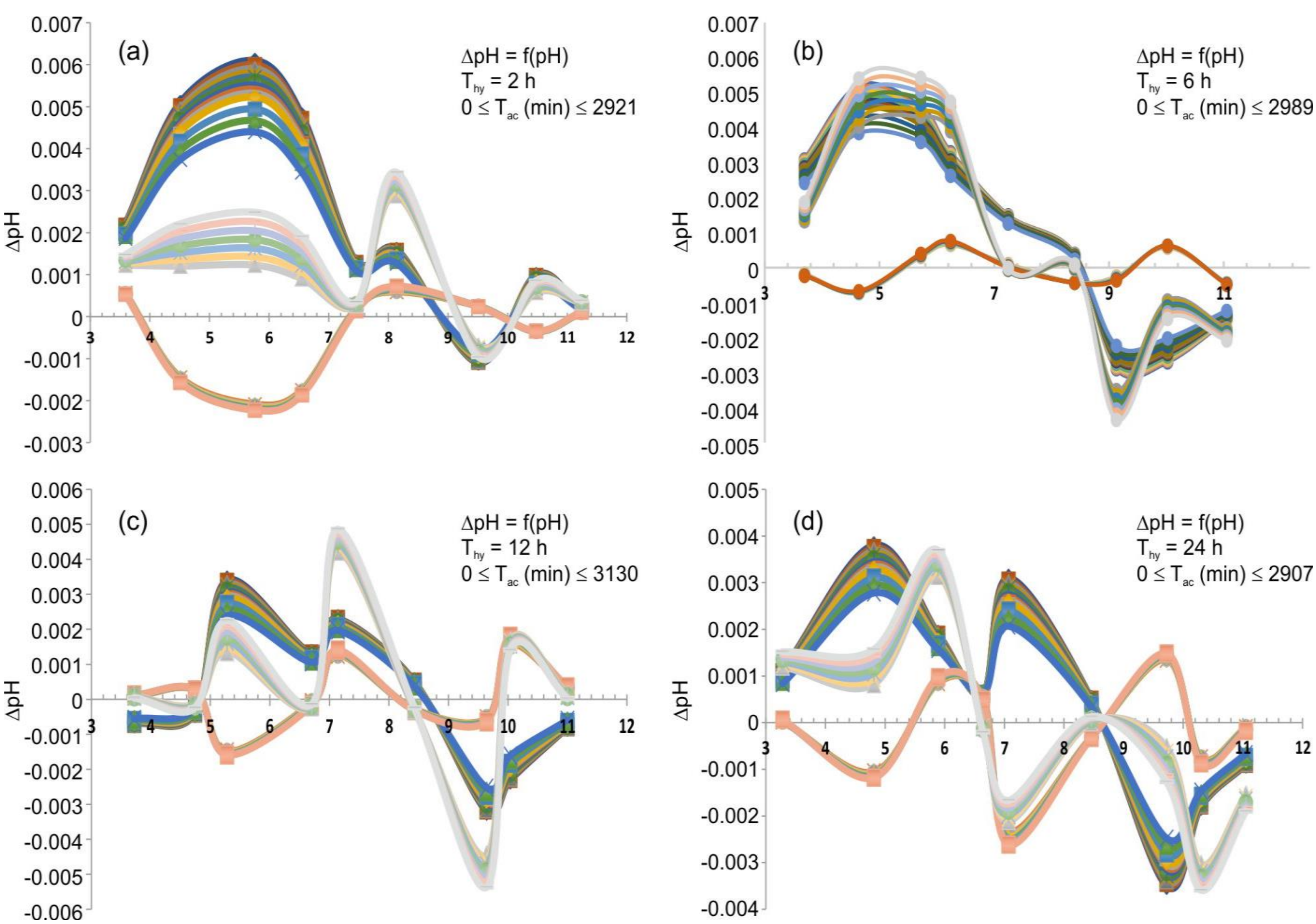

Fig. 3. Plots of varied $\Delta pH = f(pH_f)$ for natural apatite at m = 0.2 g/L: (a) $\Delta pH = f(pH)$, T_{hy} = 2 h, $0 \leq T_{ac}$ (min) ≤ 2921; (b) $\Delta pH = f(pH)$, T_{hy} = 6 h, $0 \leq T_{ac}$ (min) ≤ 2989; (c) $\Delta pH = f(pH)$, T_{hy} = 12 h, $0 \leq T_{ac}$ (min) ≤ 3130; (d) $\Delta pH = f(pH)$, T_{hy} = 24 h, $0 \leq T_{ac}$ (min) ≤ 2907

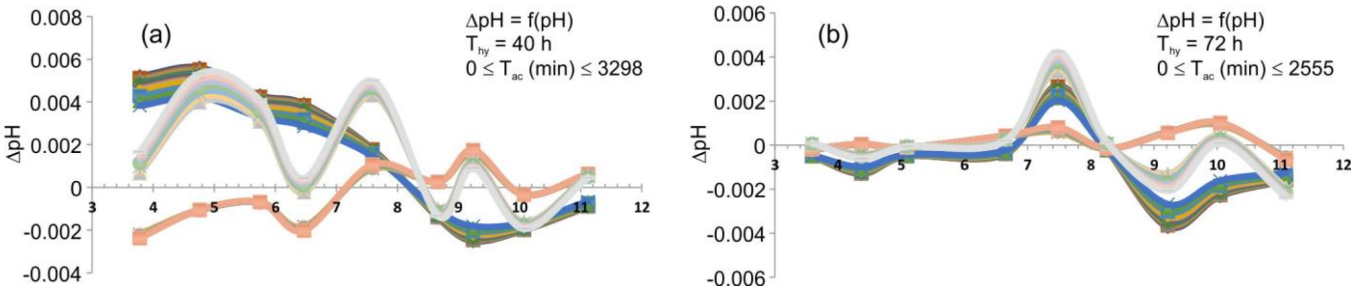

Fig. 4. Plots of varied $\Delta pH = f(pH_f)$ for natural apatite at m = 0.2 g/L: (a) $\Delta pH = f(pH)$, T_{hy} = 40 h, $0 \le T_{ac}$ (min) ≤ 329; (b) $\Delta pH = f(pH)$, T_{hy} = 72 h, $0 \le T_{ac}$ (min) ≤ 2555

for minerals such as alumina, calcite ($CaCO_3$) and sillimanite (Al_2SiO_5) [42-44]. A high IEP around pH 11.0 indicated the presence of strongly basic components like brucite or $Mg(OH)_2$. This behaviour reflects the strong affinity of $Mg(OH)_2$ surfaces for protonation under acidic conditions. Surface species such as $\overline{>MgOH_2^+}$ dominate at pH < 8 and progressively transform into neutral $\overline{>MgOH}$ and negatively charged $\overline{>MgO^-}$ species as pH increases [45-48]. Thus, the presence of multiple IEP values suggests coexistence of different reactive surface environments associated with various mineral domains. Therefore, the measured IEPs represent combined interfacial responses rather than a single homogeneous phase.

To further assess long-term hydration effects, ΔpH was also analysed as a function of activation time (T_{ac}) and hydration time for natural apatite at m = 0.2 g L^{-1} within the pH range 4.3-4.8 (Fig. 5). The results showed that the surface chemistry strongly depended on both initial pH and contact time. The relationship between pH and ΔpH was complex, reflecting rapid protonation/deprotonation reactions accompanied by release or uptake of H^+ or OH^- ions. The composition and progressive transformation of hydrated HAP were therefore strongly governed by suspension pH [49].

The surface protonation was particularly sensitive to the activation time. At initial pH values between 4.5 and 4.8, activation promoted protonation of surface hydroxyl and phosphate groups, causing a decrease in net surface charge until the point of zero charge (PZC, $\Delta pH \approx 0$) was reached after approximately 2 h [50]. This intersection point of $pH = f(T_{ac})$ also corresponded to the IEP. With further activation beyond 2 h, ΔpH increased at T_{hy} = 40 h and pH 4.5, remained nearly constant at pH 4.8 and T_{hy} = 24 h and decreased under other conditions. These findings indicate that the potentiometric measurements provide an integrated view of surface charging behaviour, where hydration, activation and mineral heterogeneity altogether control the protonation equilibria and interfacial reactivity.

Conclusion

The apatite surface can be considered as a 2D hydrated layer containing calcium and HPO_4^{2-} ions, with a variable structure depending on ionic composition. The obtained $\Delta pH = f(pH)$ results showed that both the point of zero charge (PZC) and isoelectric point (IEP) were dependent on hydration time (T_{hy}) and activation time (T_{ac}). Surface protonation/deprotonation behaviour also varied with hydration duration, indicating that interaction with water progressively modified the activated HAP surface. The hydration/activation process of apatite proceeded through complex protonation-deprotonation and hydroxylation reactions at the mineral-water interface, resulting in measurable changes in suspension pH. In particular, surface ΔpH was strongly influenced by bulk solution pH and this relationship provided useful insight into the underlying reaction mechanisms. The self-adjusting pH of the suspension influenced the conversion rates of different surface species during hydration and activation. Moreover, pH evolution was governed by the presence of associated metal oxide phases, especially those containing Si, Fe, Al, Ti, and Mg. Changes in charge distribution among reactive surface species played a key role in controlling interfacial behaviour and the morphology of precipitating brucite crystals. Thus, based on the results, this study emphasize the important role of hydration and activation pathways in determining the apatite surface reactivity.

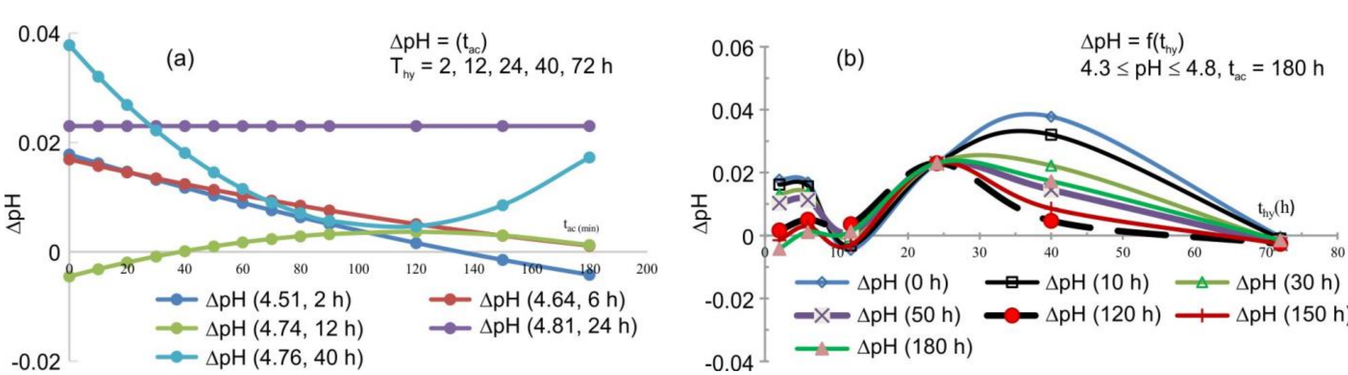

Fig. 5. Plots of varied $\Delta pH = (t_{ac}, t_{hy})$; (a) $2 \le t$ (h) ≤ 40, (b) $4.3 \le pH \le 4.8$, $t_{ac} \le 180$ h for natural apatite at m = 0.2 g/L

ACKNOWLEDGEMENTS

The authors are thankful to the authorities of University Mohamed V of Rabat for providing all the research facilities for this investigation.

CONFLICT OF INTEREST

The authors declare that there is no conflict of interests regarding the publication of this article.

DECLARATION OF AI-ASSISTED TECHNOLOGIES

During the preparation of this manuscript, the authors used an AI-assisted tool(s) to improve the language. The authors reviewed and edited the content and take full responsibility for the published work.

REFERENCES

1. G. Tchangbeddji, G. Djeteli, K.A. Kili, J.M. Savariault and J.L. Lacout, *Bull. Chem. Soc. Ethiop.*, **17**, 139 (2003); https://doi.org/10.4314/bcse.v17i2.61659
2. M. Okada and T. Matsumoto, *Jpn. Dent. Sci. Rev.*, **51**, 85 (2015); https://doi.org/10.1016/j.jdsr.2015.03.004
3. N. Subramanian and L.N. Lammers, *J. Colloid Interface Sci.*, **608**, 692 (2022); https://doi.org/10.1016/j.jcis.2021.09.106
4. M.A. Henderson, *Surf. Sci. Rep.*, **46**, 1 (2002); https://doi.org/10.1016/S0167-5729(01)00020-6
5. K. Andersson, PhD Thesis, Structure, Bonding and Chemistry of Water and Hydroxyl on Transition Metal Surfaces, Stockholm University, Stockholm, p. 62 (2006).
6. E. Brini, C.J. Fennell, M. Fernandez-Serra, B. Hribar-Lee, M. Lukšič and K.A. Dill, *Chem. Rev.*, **117**, 12385 (2017); https://doi.org/10.1021/acs.chemrev.7b00259
7. R. Singh, in eds.: M.S. Liew, P. Nguyen-Tri, T.A. Nguyen and S. Kakooei, Smart Nano Concretes and Cement-Based Materials: Properties, Modelling and Applications, Elsevier, Amsterdam, pp. 157-182 (2020); https://doi.org/10.1016/B978-0-12-817854-6.00006-4
8. E.C. Donaldson, G.V. Chilingarian and T.F. Yen, *Adv. Colloid Interface Sci.*, **134-135**, 57 (2008); https://doi.org/10.1016/C2013-0-15527-4
9. P. Fenter and N.C. Sturchio, *Prog. Surf. Sci.*, **77**, 171 (2004); https://doi.org/10.1016/j.progsurf.2004.12.001
10. E. Lee, *Interface Sci. Technol.*, **26**, 3 (2019); https://doi.org/10.1016/B978-0-08-100865-2.00001-1
11. C.M. Schott, P.M. Schneider, K.-T. Song, H. Yu, R. Götz, F. Haimerl, E. Gubanova, J. Zhou, T.O. Schmidt, Q. Zhang, V. Alexandrov and A.S. Bandarenka, *Chem. Rev.*, **124**, 12391 (2024); https://doi.org/10.1021/acs.chemrev.3c00806
12. L. Bertinetti, C. Drouet, C. Combes, C. Rey, A. Tampieri, S. Coluccia and G. Martra, *Langmuir*, **25**, 5647 (2009); https://doi.org/10.1021/la804230j
13. F. Min, C. Peng and S. Song, *Arch. Min. Sci.*, **59**, 489 (2014); https://doi.org/10.2478/amsc-2014-0035
14. W. Zheng, C. Sun and B. Bai, *Polymers*, **9**, 370 (2017); https://doi.org/10.3390/polym9080370
15. T.K. Shimizu, S. Maier, A. Verdaguer, J.J. Velasco-Velez and M. Salmeron, *Prog. Surf. Sci.*, **93**, 87 (2018); https://doi.org/10.1016/j.progsurf.2018.09.004
16. C. Xiao, P. Shi, W. Yan, L. Chen, L. Qian and S.H. Kim, *Colloids Interfaces*, **3**, 55 (2019); https://doi.org/10.3390/colloids3030055
17. A.J. Rieth, K.M. Hunter, M. Dincă and F. Paesani, *Nat. Commun.*, **10**, 4771 (2019); https://doi.org/10.1038/s41467-019-12751-z
18. D. Eichert, C. Combes, C. Drouet and C. Rey, *Key Eng. Mater.*, **284–286**, 3 (2005); https://doi.org/10.4028/www.scientific.net/KEM.284-286.3
19. C. Combes, S. Cazalbou and C. Rey, *Minerals*, **6**, 34 (2016); https://doi.org/10.3390/min6020034
20. M. Ibrahim, M. Labaki, J.-M. Giraudon and J.-F. Lamonier, *J. Hazard. Mater.*, **383**, 121139 (2020); https://doi.org/10.1016/j.jhazmat.2019.121139
21. M. Gruselle, K. Tõnsuaadu, P. Gredin and C. Len, *Mol. Catal.*, **519**, 112146 (2022); https://doi.org/10.1016/j.mcat.2022.112146
22. K. Kandori, S. Oda, M. Fukusumi and Y. Morisada, *Colloids Surf. B Biointerfaces*, **73**, 140 (2009); https://doi.org/10.1016/j.colsurfb.2009.05.011
23. T. Tsuchida, J. Kubo, T. Yoshioka, S. Sakuma, T. Takeguchi and W. Ueda, *J. Catal.*, **259**, 183 (2008); https://doi.org/10.1016/j.jcat.2008.08.005
24. I.D. Smičiklas, S.K. Milonjić, P. Pfendt and S. Raičević, *Sep. Purif. Technol.*, **18**, 185 (2000); https://doi.org/10.1016/S1383-5866(99)00066-0
25. T. Saito, T. Yokoi, A. Nakamura and K. Matsunaga, *RSC Adv.*, **11**, 34004 (2021); https://doi.org/10.1039/D1RA06311A
26. B. Sawangjang, P. Induvesa, A. Wongrueng, C. Pumas, S. Wattanachira, P. Rakruam, P. Punyapalakul, S. Takizawa and E. Khan, *Int. J. Environ. Res. Public Health*, **18**, 6878 (2021); https://doi.org/10.3390/ijerph18136878
27. M. Kosmulski, *Adv. Colloid Interface Sci.*, **296**, 102519 (2021); https://doi.org/10.1016/j.cis.2021.102519
28. E. Skwarek, W. Janusz and D. Sternik, *J. Radioanal. Nucl. Chem.*, **299**, 2027 (2013); https://doi.org/10.1007/s10967-013-2825-z
29. L. Bilali, M. Benchanaa, K. El Harfi, A. Mokhlisse and A. Outzourhit, *J. Anal. Appl. Pyrolysis*, **73**, 1 (2005); https://doi.org/10.1016/j.jaap.2004.08.004
30. L. Bilali, M. Benchanaa, A. Outzourhit and A. Mokhlisse, *J. Microw. Power Electromagn. Energy*, **43**, 31 (2008); https://doi.org/10.1080/08327823.2008.11688608
31. C.L. Owens, G.R. Nash, K. Hadler, R.S. Fitzpatrick, C.G. Anderson and F. Wall, *Adv. Colloid Interface Sci.*, **265**, 14 (2019); https://doi.org/10.1016/j.cis.2019.01.004
32. S. Singh and S. Jonnalagadda, *Bull. Chem. Soc. Ethiop.*, **27**, 57 (2013); https://doi.org/10.4314/bcse.v27i1.6
33. F.-E. Maarouf, S. Saoiabi, K. Azzaoui, H. Khalil, A.E. Yahyaoui, M. Khalil, A. Saoiabi, B. Hammouti, M.H. Youssoufi, S. Shityakov, O. Hamed, S. Jodeh and R. Sabbahi, *Indones. J. Sci. Technol.*, **7**, 187 (2022); https://doi.org/10.17509/ijost.v7i2.45948
34. H. Khalil, F.E. Maarouf, M. Khalil, S. Saoiabi, M. Hmamou, K. Azzaoui, A. Saoiabi and B. Ammary, *Biointerface Res. Appl. Chem.*, **13**, 205 (2022); https://doi.org/10.33263/BRIAC133.205
35. F.Z. Maarouf, S. Saoiabi, K. Azzaoui, C. Chrika, H. Khalil, S. Elkaouni, S. Lhimr, O. Boubker, B. Hammouti and S. Jodeh, *MC Chem.*, **15**, 48 (2021); https://doi.org/10.1186/s13065021-00774-x
36. P. Somasundaran, *J. Colloid Interface Sci.*, **27**, 659 (1968); https://doi.org/10.1016/0021-9797(68)90098-2
37. M. Kosmulski, *Adv. Colloid Interface Sci.*, **319**, 102973 (2023); https://doi.org/10.1016/j.cis.2023.102973
38. E.M. Pecini and M.J. Avena, *Langmuir*, **29**, 14926 (2013); https://doi.org/10.1021/la403384g
39. G. Fan, L. Wang, Y. Cao and C. Li, *Minerals*, **10**, 681 (2020); https://doi.org/10.3390/min10080681
40. C.M. Jonsson, C.L. Jonsson, C. Estrada, D.A. Sverjensky, H.J. Cleaves II and R.M. Hazen, *Geochim. Cosmochim. Acta*, **74**, 2356 (2010); https://doi.org/10.1016/j.gca.2010.01.003
41. L. Xie, J. Wang, Q. Lu, W. Hu, D. Yang, C. Qiao, X. Peng, Q. Peng, T. Wang, W. Sun, Q. Liu, H. Zhang and H. Zeng, *Adv. Colloid Interface Sci.*, **295**, 102491 (2021); https://doi.org/10.1016/j.cis.2021.102491
42. S.K. Mishra, *Int. J. Miner. Process.*, **5**, 69 (1978); https://doi.org/10.1016/0301-7516(78)90006-6
43. A.L. Martínez and A.S. Uribe, *Miner. Eng.*, **8**, 1009 (1995); https://doi.org/10.1016/0892-6875(95)00064-W

44. M. Derhy, Y. Taha, R. Hakkou and M. Benzaazoua, *Minerals*, **10**, 1109 (2020); https://doi.org/10.3390/min10121109
45. H. Schott, *J. Pharm. Sci.*, **70**, 486 (1981); https://doi.org/10.1002/jps.2600700505
46. O.S. Pokrovsky and J. Schott, *Geochim. Cosmochim. Acta*, **68**, 31 (2004); https://doi.org/10.1016/S0016-7037(03)00238-2
47. T.W. Healy and D.W. Fuerstenau, *J. Colloid Interface Sci.*, **309**, 183 (2007); https://doi.org/10.1016/j.jcis.2007.01.048
48. M. Pettauer, A. Baldermann, S. Eder and M. Dietzel, *Cryst. Growth Des.*, **24**, 3085 (2024); https://doi.org/10.1021/acs.cgd.4c00243
49. P. Zhang and J.A. Ryan, *Environ. Sci. Technol.*, **33**, 625 (1999); https://doi.org/10.1021/es980268e
50. P. Molle, A. Liénard, A. Grasmick, A. Iwema and A. Kabbabi, *Water Sci. Technol.*, **51**, 193 (2005); https://doi.org/10.2166/wst.2005.0318